Polarization properties and dispersion relations for spiral resonances of a dielectric rod

Harald G. L. Schwefel and A. Douglas Stone*
Yale University, Department of Applied Physics,
P.O. Box 208284, New Haven, CT 06520-8284, USA

Hakan E. Tureci
Yale University, Department of Physics,
P.O. Box 208120, New Haven,
CT 06520-8120, USA

Dielectric microcavities based on cylindrical and deformed cylindrical shapes have been employed as resonators for microlasers. Such systems support spiral resonances with finite momentum along the cylinder axis. For such modes the boundary conditions do not separate and simple TM and TE polarization states do not exist. We formulate a theory for the dispersion relations and polarization properties of such resonances for an infinite dielectric rod of arbitrary cross-section and then solve for these quantities for the case of a circular cross-section (cylinder). Useful analytic formulas are obtained using the eikonal (Einstein-Brillouin-Keller) method which are shown to be excellent approximations to the exact results from the wave equation. The major finding is that the polarization of the radiation emitted into the far-field is linear up to a polarization critical angle (PCA) at which it changes to elliptical. The PCA always lies between the Brewster and total-internal-reflection angles for the dielectric, as is shown by an analysis based on the Jones matrices of the spiraling rays.

OCIS codes: 060.2310,260.5740,260.5430,080.2720

1. Introduction

There has been a great deal of recent interest in cylindrical and deformed cylindrical dielectric resonators for micro-laser applications.[1–5] From the theory side there is a particular interest in the deformed case, as in this case such resonators are wave-chaotic systems and can be analyzed with methods from non-linear dynamics and semi-classical quantum theory. Analysis of the resonances and emission patterns from such systems has focused exclusively on the scalar Helmholtz equation which describes the axial component of the electric (TM mode) or magnetic (TE mode) fields for the case of resonant modes with zero momentum in the axial direction (z-direction). For this case ($k_z = 0$) the polarization state is unchanged by boundary scattering and the non-trivial ray dynamics in the transverse plane does not affect the polarization state of the resonant solutions. However it is interesting to consider the solutions of the wave equation for both cylindrical and deformed cylindrical dielectric rods with $k_z \neq 0$, since in this case the boundary scattering couples the electric and magnetic fields and there no longer exist TM or TE solutions with a fixed direction in space for one the fields. We refer to these non-zero k_z modes as "spiral modes" and note that elastic scattering from such spiral resonance modes has been measured previously by Poon et al. Ref. 6, the polarization properties were unfortunately fully explored in those experiments.

The authors did however measure a systematic "blue-shift" of the resonance modes with tilt angle, which has been predicted by Ref. 7,8 and which we will derive below. The modes we study here are similar to the hybrid modes known in the study of optical fibers, where it is also well-known that there are no simple TE, TM or TEM-like modes, but more complex vector solutions are necessary. Our emphasis differs however in several ways: 1) we are interested in uniform dielectric rods, not the variable index profiles typical of optical fibers. 2) We are interested in modes which are not totally internally reflected so we can study the nature of the polarization of the emitted radiation in the far-field. 3) We are primarily interested in resonances of uniform rods with cross-sections in the range of tens to hundreds of μm, so they are strongly multi-mode and can be treated within the eikonal (semi-classical) approximation.

Here, we will model finite resonators as infinite dielectric rods, neglecting the end effects in the z-direction; we therefore formulate the vector wave equation and the necessary boundary conditions for an infinite rod of arbitrary cross-section. Various approximations are possible to treat end effects when they are relevant, but we will not explore them here. We define the resonant solutions

*Electronic address: Harald.Schwefel@yale.edu

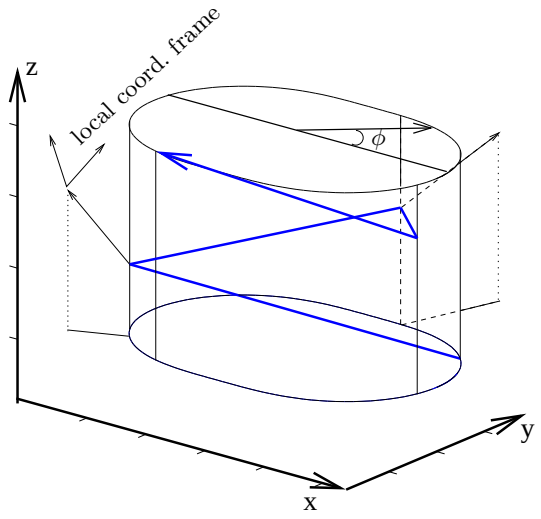

Fig. 1. Schematics of a spiraling ray in a rod with arbitrary cross-section. The ray can refract out and the polarization can be defined in the far-field with respect to a local coordinate system. For a general deformation, the polarization will change with the azimuthal angle ϕ. Here, we will focus only on the circular cross-section, where the polarization is constant (with respect to ϕ) when referred to the local coordinate system oriented along and perpendicular to a ray in the far-field.

(quasi-bound modes) of such a system and write down a general formalism which can be used to obtain exact numerical solutions for the vector resonances. We also show how the corresponding solutions can be used to derive the spatially-varying polarization state of the emitted radiation in the far-field. We then study in detail these equations in the case of a circular cross-section (cylinder) for which a great deal of analytic progress and physical insight may be obtained. The analysis of the non-circular case for which wave-chaotic polarization states are possible will be published elsewhere.[9]

Our goal is to relate the polarization state in the far-field to the projected two-dimensional ray motion in the plane transverse to the z-axis. (See Fig. 1) One can have spiral resonances which range from motion along the diameter of the rod in the transverse plane (bouncing ball type modes) to whispering gallery modes which circulate around the perimeter of the rod as they spiral along it. We will discuss how the polarization properties of the resonances vary as the angle of incidence in the plane ($\sin\chi$) and the spiral (tilt) angle (θ) with respect to the $x-y$ plane varies. (In Fig. 2 A) we introduce the relevant geometric parameters.) It should be noted that due to the curvature of the boundary, even modes which are totally-internally reflected according to geometric optics do emit by evanescent radiation into the far-field and their polarization fields can be obtained from exact solution of the wave equation, although experimentally it may be impractical to measure their weak emission far above the critical angle. In the simplest case of $k_z = 0$ ($\theta = 0$) one finds pure linear polarization in the far-field; in addition, the resonant energies are just those of the two-dimensional problem of a dielectric disk. In this two-dimensional case the resonant energies in the semiclassical limit are determined by the optical path length as well as by the phase shifts due to caustics and reflections at the boundary.[10] These boundary terms in the semiclassical limit correspond simply to the TIR phase shifts for TM and TE scattering off a plane dielectric interface when $\sin\chi > \sin\chi_c = 1/n$ (here n is the index of refraction of the rod surrounded by air); if $\sin\chi < \sin\chi_c = 1/n$ there is zero phase shift but just a loss (imaginary part of k) given by the Fresnel scattering coefficients. For the spiral modes ($k_z \neq 0$), the boundary terms have a new character corresponding neither to the TE nor to the TM Fresnel scattering and new phenomena can occur, such as a non-zero phase shift for modes which are not TIR. We derive below the generalization of the Fresnel scattering coefficients for spiral modes of the cylinder using the vector eikonal method. We find that the angle at which a non-zero phase shift sets in is always between the critical angle and the Brewster angle and coincides precisely with the onset of elliptical polarization in the far-field. We call this new key quantity the polarization critical angle (PCA)

In Section 2 of the paper we set up the relevant form of the vector wave equations for the infinite dielectric rod and formulate the boundary conditions for the quasi-bound modes (resonances). In Section 3 we discuss how to extract the far-field polarization of these quasi-bound modes. All results are for the general case of arbitrary cross-section of the rod. In Section 4 we specialize to the case of the dielectric cylinder and reduce the resonance problem to a simple root-finding problem. This equation is exact and is shown to yield the systematic blue-shift in Ref. 6. In Section 5 we reformulate the same problem using the eikonal (EBK) method which yields a simpler analytic formula for the resonances and allows a statement of the polarization problem in terms of generalized Fresnel coefficients. The exact and EBK resonance wavevectors are shown to agree quite well, down to small k. In Section 6 we restate the polarization problem in terms of Jones matrices and thus derive the internal polarization state and the farfield polarization of the resonances in the semi-classical limit. Both the Jones and EBK formulations are shown to yield the same answer for this quantity and to agree with the exact results to a good approximation. Finally, the origin of the polarization critical angle is explained.

2. Wave equation and resonances for the infinite dielectric rod

For electromagnetic fields in free space interacting with uniform dielectrics, Maxwell equations reduce to the *vec-*

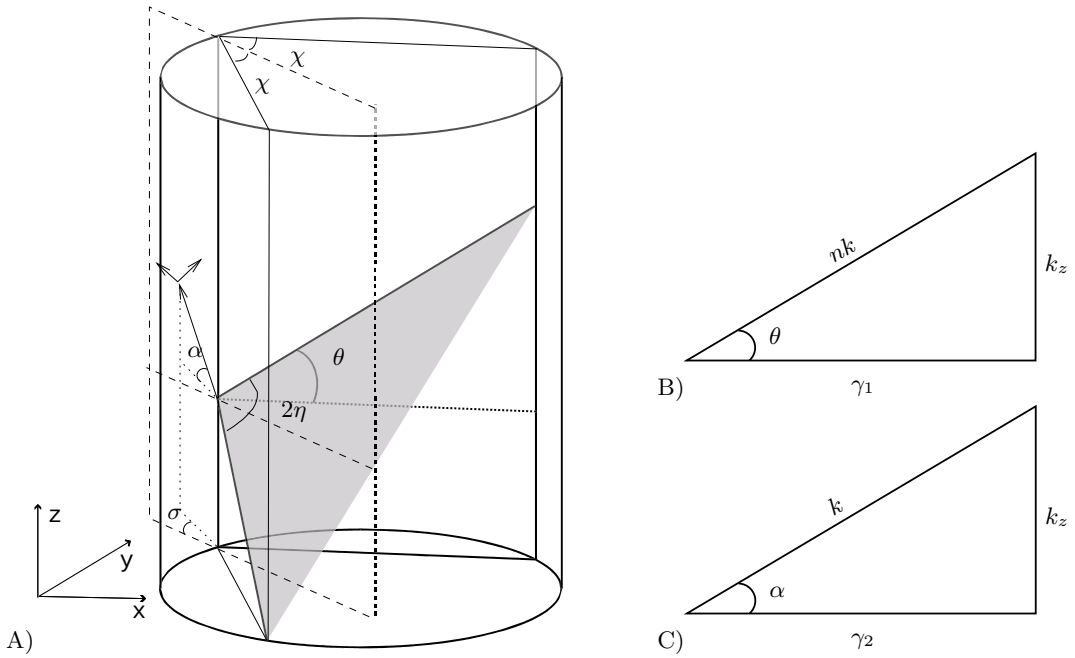

Fig. 2. A) Coordinates used for ray dynamics in a rod with arbitrary cross-section. The ray can refract out and the polarization can be defined in the far-field with respect to a local cartesian coordinate system tilted so that one of the axes is along the propagation direction. We define η as the angle of incidence in the plane of incidence; χ, the angle of incidence projected into the plane; σ, the projected far-field angle; θ, the tilt angle measured from the cross-sectional $x-y$ plane, given by $\tan\theta = k_z/\gamma_1$; α, the external tilt angle $\tan\alpha = k_z/\gamma_2$; B), C) Schematics highlighting the trigonometric relations among the inside and outside quantities. Note that α can be found through the application of Snell's law, $n\sin\theta = \sin\alpha$.

tor Helmholtz equation

$$\left(\nabla^2 + n^2k^2\right)\begin{Bmatrix}\boldsymbol{E}(x,y,z)\\ \boldsymbol{B}(x,y,z)\end{Bmatrix} = 0, \tag{1}$$

where n is the uniform index of the rod and $n = 1$ outside the rod. Thus n differs from unity in an arbitrary closed simply-connected domain ∂D in the $x-y$ plane for all values of z (the rod is infinite in the z-direction). The translational symmetry along the z-axis (see Fig. 1) allows us to express the z-variation of the fields as

$$\boldsymbol{E}(\boldsymbol{x}) = \boldsymbol{E}(x,y)\mathrm{e}^{-ik_z z}, \quad \boldsymbol{B}(\boldsymbol{x}) = \boldsymbol{B}(x,y)\mathrm{e}^{-ik_z z}; \tag{2}$$

and henceforth the vectors $\boldsymbol{E}, \boldsymbol{B}$ will refer to the x, y dependent vector fields just defined. With this ansatz, we can show that the most general solution of the six-component vector wave equation for this problem is determined by E_z and B_z components alone; the perpendicular fields are given by linear combinations of these two scalar fields and their derivatives.[11] Hence we must solve the two-component scalar wave equation

$$\left(\nabla^2 + \gamma^2\right)\begin{Bmatrix}E_z(x,y)\\ B_z(x,y)\end{Bmatrix} = 0, \quad \text{with} \quad \gamma^2 = n(\boldsymbol{x})^2k^2 - k_z^2, \tag{3}$$

where we have introduced the *reduced wavevector* γ which is the wavevector associated with the transverse motion. The complication of solving this remaining two-component Helmholtz equation stems from the fact that the two fields E_z, B_z are coupled through the *boundary conditions*. Four independent boundary conditions are found through the application of the general Maxwell boundary conditions:

$$E_{z1} = E_{z2} \quad \text{or} \quad \partial_t E_{z1} = \partial_t E_{z2} \tag{4}$$

$$B_{z1} = B_{z2} \quad \text{or} \quad \partial_t B_{z1} = \partial_t B_{z2} \tag{5}$$

$$\frac{k}{\gamma_1^2}\partial_n B_{z1} - \frac{k}{\gamma_2^2}\partial_n B_{z2} = -\left(\frac{k_z}{\gamma_1^2} - \frac{k_z}{\gamma_2^2}\right)\partial_t E_{z1} \tag{6}$$

$$\frac{n_1^2 k}{\gamma_1^2}\partial_n E_{z1} - \frac{n_2^2 k}{\gamma_2^2}\partial_n E_{z2} = +\left(\frac{k_z}{\gamma_1^2} - \frac{k_z}{\gamma_2^2}\right)\partial_t B_{z1}. \tag{7}$$

Here, 1 and 2 refer to inside and outside solutions. We recover the familiar special case of two-dimensional modes when we take $k_z = 0$; in this case the boundary conditions can be satisfied with either $B_z = 0$ (TM solutions) or $E_z = 0$ (TE solutions) i.e. we get spatially uniform eigenpolarization directions. For the TM case we find

$\boldsymbol{E}_\perp = 0$ and

$$\boldsymbol{B}_\perp = \frac{i}{\gamma^2} n^2 k \begin{pmatrix} -\partial_y E_z \\ \partial_x E_z \end{pmatrix} \tag{8}$$

and for the TE case we find $\boldsymbol{B}_\perp = 0$ and

$$\boldsymbol{E}_\perp = -\frac{i}{\gamma^2} k \begin{pmatrix} -\partial_y B_z \\ \partial_x B_z \end{pmatrix}. \tag{9}$$

In both cases the equations Eqs. (4)-(7) completely decouple and we have only to solve the scalar Helmholtz equation for E_z or B_z with the boundary conditions of the continuity of the field and its normal derivative on the boundary. In both cases the electromagnetic field is linearly polarized in the far-field, either in the direction parallel to the rod axis (TM) or perpendicular to it (TE). We will now focus on the $k_z \neq 0$ modes which we will refer to as spiral modes. We will not consider the extreme case where $k = k_z$ (TEM modes).

Our interest is in the dielectric rod as a resonator, i.e. as a device for trapping light. Experiments on resonators fall into two broad categories, and the presence of quasi-bound modes are manifested differently in these two situations. One can measure elastic scattering of incident laser light from such a rod, as was done in Ref. 6 and focus on the specific wavevectors at which one observes scattering resonances. For this case the linear wave equation that we are studying provides an exact description. One can also imagine the rod containing a gain medium and when pumped emitting laser light into these spiral resonances.[10] In such a case, the linear wave equation is not an exact description; however for high-Q resonances typically the resonances of the passive and active cavity are very similar.[12] In order for the laser to emit specifically into spiral modes, there would have to be some mechanism to suppress lasing of planar ($k_z = 0$) modes; one could imagine doing this with a small seed pump which is tuned to the frequency of a spiral mode and pushes it above threshold before all the other modes. It is possible to describe these two different physical situations (elastic scattering and lasing) using appropriate boundary conditions on the linear vector Helmholtz equation. To be precise, we assume that the rod is bounded by the interface ∂D given by (see Fig. 1)

$$\partial D = R(z,\phi) \quad \forall \quad z \in \mathbb{R}, \quad \phi \in [0, 2\pi]. \tag{10}$$

We are typically interested in boundaries which are smooth and not too far from a circle, hence it is natural to expand the internal and external solutions E_z and B_z of Eq. (3) in cylindrical harmonics[13]

$$\begin{pmatrix} E_z^< \\ B_z^< \end{pmatrix} = \sum_{m=-\infty}^{\infty} \left[\begin{pmatrix} \alpha_m \\ \xi_m \end{pmatrix} H_m^+(\gamma_1 r) + \begin{pmatrix} \beta_m \\ \eta_m \end{pmatrix} H_m^-(\gamma_1 r) \right] e^{im\phi} \tag{11}$$

$$\begin{pmatrix} E_z^> \\ B_z^> \end{pmatrix} = \sum_{m=-\infty}^{\infty} \left[\begin{pmatrix} \upsilon_m \\ \zeta_m \end{pmatrix} H_m^+(\gamma_2 r) + \begin{pmatrix} \delta_m \\ \vartheta_m \end{pmatrix} H_m^-(\gamma_2 r) \right] e^{im\phi}, \tag{12}$$

where $H^\pm$ are the Hankel-functions, H^- representing an incoming wave from infinity and H^+ an outgoing wave.

To describe the scattering experiment we simply apply the boundary conditions Eqs. (4)-(7) which will connect these interior and exterior solutions by a set of linear equations for the coefficients $\alpha_m, \xi_m, \ldots, \vartheta_m$. These linear equations will have solutions for any incident wavevector k and will define a scattering matrix for the fields which can be used to calculate the intensity scattered at any given far-field angle. An example of such a calculation for the cylinder is given in Fig. 3; the values of kR (R is the cylinder radius) at which rapid variation is observed are the resonant wavevectors for which the incident light is trapped for long periods. However the precise pattern of radiation in the far-field in this case is determined by both the scattered and incident radiation and is not representative of a lasing mode for which there is no incident radiation. To determine the resonances corresponding to emission from a source it is conventional to use the Sommerfeld or radiation boundary conditions; in this case we would set the incident waves from outside to zero (the coefficients δ_m, ϑ_m in Eq. (12)) and still impose the boundary conditions of Eqs. (4)-(7). The resulting linear equations for the remaining coefficients would not have any solutions for real k (since current is not conserved), but would have discrete solutions for complex k values; those solutions are known as the quasi-bound modes of the problem. It can be shown that the discrete complex solutions of this problem correspond to the poles of the S-matrix of the current-conserving problem when that S-matrix is continued to complex values of k (see e.g. Ref. 10,13). $\mathrm{Re}\,[k]$ at the pole position gives the approximate location of the resonant peak in the on-shell S-matrix and the $\mathrm{Im}\,[k]$ gives the width of the peak; the Q-value of the resonance is just $Q = 2\mathrm{Re}\,[k]\,/|\mathrm{Im}\,[k]\,|$. These statements hold for $k_z = 0$ resonances; for the spiral modes there are solutions for all k_z and for discrete complex values of the reduced wavevector γ. Once the resonant wavevector has been found the coefficients of the outgoing waves can be determined to give the emission pattern and polarization properties of the emitted radiation. As is well-known, the Hankel functions with complex k and large argument grow exponentially and do not provide normalizable fields at infinity. This is unimportant for studying the emission patterns as a function of far-field angle or polarization properties, although it may cause some practical difficulties in numerical algorithms. If desired, this unphysical feature of the solutions can be avoided for a given resonance by adding a tunable imaginary part of the index of refraction to yield a solution with real k outside the dielectric. This imaginary part represents linear amplification in the medium and would give an estimate for the lasing threshold for that mode if mode competition effects were negligible. One finds that these real k solutions are continuously related to the complex k quasi-bound states at real index and have approximately the same spatial properties except for the absence of growth at infinity.

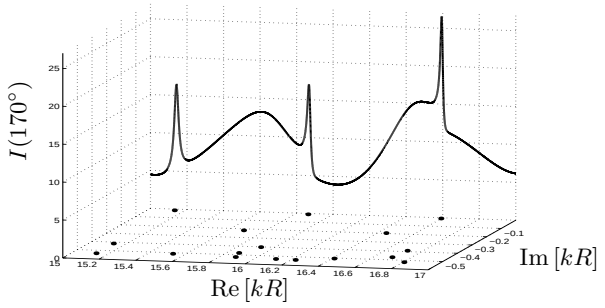

Fig. 3. A comparison of scattering and emission pictures for quasi-bound modes. The complex quasi-bound mode frequencies are plotted on the $\mathrm{Re}\,[kR] - \mathrm{Im}\,[kR]$ plane. On the back panel we plot the real k S-matrix, scattering cross-section at 170° with respect to the incoming wave direction. Notice that the most prominent peaks in scattering intensity are found at the values of k where a quasi-bound mode frequency is closest to the real-axis. These are the long-lived resonances of the cavity. Also visible is the contribution of resonances with shorter lifetimes (higher values of $\mathrm{Im}\,[kR]$) to broader peaks and the scattering background. Calculations are for a dielectric cylinder with $n = 1.5$ and for $k_z = 0$.

3. Polarization of spiral modes in the far-field

Having outlined how to solve for the quasi-bound spiral modes we now analyze their polarization properties. Strictly speaking polarization of the time-harmonic electromagnetic field cannot be defined inside the cavity or in the near field around it as the electric and magnetic fields need not be perpendicular to one another or to the direction of energy flow. In the far-field on the other hand, where the radiation is well-approximated locally by a plane wave, we should be able to analyze the polarization of the emission from spiral modes in conventional terms. Assuming the matching problem is solved, the coefficients υ_m, ζ_m determining $E_z^<(\rho,\varphi), B_z^<(\rho,\varphi)$ are known and these fields can be differentiated in order to find $\boldsymbol{E}_\perp$ everywhere outside the rod. These relations simplify if we use the large argument expansion of the Hankel functions and their recursion relations to find the relative magnitudes of the $\boldsymbol{E}$-field components in cylindrical coordinates as $\rho \to \infty$,

$$\left|\begin{pmatrix} E_\rho \\ E_\varphi \\ E_z \end{pmatrix}\right|^2 \sim \left|\begin{pmatrix} k_z/\gamma_2 \sum \upsilon_m e^{im(\varphi-\pi/2)} \\ k/\gamma_2 \sum \zeta_m e^{im(\varphi-\pi/2)} \\ \sum \upsilon_m e^{im(\varphi-\pi/2)} \end{pmatrix}\right|^2 = \left|\begin{pmatrix} k_z/\gamma_2 E_z \\ k/\gamma_2 B_z \\ E_z \end{pmatrix}\right|^2 \tag{13}$$

To extract the polarization at a particular angular direction φ we need to recognize that far away from the rod the radiation is not propagating in the radial (ρ) direction with respect to the cylindrical coordinates centered on the rod axis but is instead propagating at angle α between the ρ and z directions determined by Snell's law for the z motion (See Fig. 2). We can then rotate our coordinate system by α

$$\begin{pmatrix} \cos\alpha & 0 & -\sin\alpha \\ 0 & 1 & 0 \\ \sin\alpha & 0 & \cos\alpha \end{pmatrix} \begin{pmatrix} \tan\alpha E_z \\ \sec\alpha B_z \\ E_z \end{pmatrix} = \begin{pmatrix} 0 \\ \sec\alpha B_z \\ \sec\alpha E_z \end{pmatrix}. \tag{14}$$

In this rotated coordinate system in the farfield, the electric field (on the RHS) only has two components in the plane transverse to the propagation direction. Thus, the polarization of the electric field in the far-field is then determined by the ratio of these two components, $E_z(\varphi)/B_z(\varphi)$. If these two field amplitudes have zero phase difference we have linear polarization in a certain direction which can vary as the angle of observation φ varies; if there is a non-zero phase shift Δ between them, then we typically have elliptical polarization except in the specific case of $\Delta = \pi/2$ and $|B_z|^2 = |E_z|^2$ corresponding to circular polarization. It should be noted that when the angle α is complex $k_z > k$ then the wavevector γ_2 of the outgoing Hankel functions is pure imaginary and there is no propagating radiation as $\rho \to \infty$; this corresponds to the total internal reflection condition with respect to the z motion of internal ray in the cylinder, $n \sin\theta = 1$ (see Fig. 2), for which there is no evanescent escape. It should be emphasized however that this does not correspond to the true total reflection condition for spiraling rays, which comes at smaller θ except in the case of normal incidence in the transverse plane. In particular one can ask about the polarization states in the far-field of spiral whispering gallery modes, which emit solely by evanescent escape.

The analysis up to this point has been exact for a dielectric rod of arbitrary cross-section and the various formulas can be used to solve for both the resonance wavevectors and polarization properties of the spiral modes of such a system. We have developed and implemented a numerical algorithm to do this[11]; we intend to describe the algorithm and present results for deformed cylinders in a subsequent paper.[9] At this point we specialize to the problem of spiral modes of a cylinder for which a number of analytic techniques are possible which will allow us to develop a useful physical picture.

4. Quasi-bound resonances in the cylinder

Focusing now on the case of the cylinder (circular cross-section) we have the immediate simplification that the Helmholtz equation and boundary conditions separate in cylindrical coordinates and we can look for solutions corresponding to a single component of the angular momentum, m, instead of the sums in Eq. 11. In the following we will use the following notation:

$$J_m := J_m(\gamma_1 R) \quad \text{and} \quad H_m := H_m^+(\gamma_2 R) \tag{15}$$

where $\gamma_i = \sqrt{n_i^2 k^2 - k_z^2}, i \in \{1,2\}$ and R is taken on the boundary of the domain. With this convention we can

write the ansatz for the cylinder

$$E_z^<(\boldsymbol{r};m,j) = \alpha_m J_m(\gamma_1^{m,j}\boldsymbol{r})e^{im\varphi} \qquad \boldsymbol{r} < R \tag{16}$$
$$B_z^<(\boldsymbol{r};m,j) = \xi_m J_m(\gamma_1^{m,j}\boldsymbol{r})e^{im\varphi} \qquad \boldsymbol{r} < R \tag{17}$$
$$E_z^>(\boldsymbol{r};m,j) = \upsilon_m H_m^+(\gamma_2^{m,j}\boldsymbol{r})e^{im\varphi} \qquad \boldsymbol{r} > R \tag{18}$$
$$B_z^>(\boldsymbol{r};m,j) = \zeta_m H_m^+(\gamma_2^{m,j}\boldsymbol{r})e^{im\varphi} \qquad \boldsymbol{r} > R. \tag{19}$$

Here, j is the radial mode index enumerating the solutions for a given m. Using the boundary conditions for the continuity of the field, Eqs. (4) and (5), we get the relations

$$\upsilon_m = \frac{J_m}{H_m}\alpha_m \qquad \zeta_m = \frac{J_m}{H_m}\xi_m. \tag{20}$$

Using this, Eqs. (6) and (7) can be rewritten in the following form

$$\begin{pmatrix} im(n-n^3)\sin\theta J_m H_m & \cos^2\alpha\, H_m\partial_\rho J_m - n^2\cos^2\theta\, J_m\partial_\rho H_m \\ n^2\cos^2\alpha\, H_m\partial_\rho J_m - n^2\cos^2\theta\, J_m\partial_\rho H_m & im(n^3-n)\sin\theta J_m H_m \end{pmatrix}\begin{pmatrix}\alpha_m \\ \xi_m\end{pmatrix} = 0, \tag{21}$$

where the angles are given following the convention in Fig. 2 B), C), with $\tan\theta = k_z/\gamma_1$. θ is the interior angle of the ray spiraling up with respect to the (x,y) plane and α the corresponding exterior angle. In order for this system to have a non-trivial solution the determinant needs to vanish, resulting in:

$$\begin{aligned}(1-n^2)^2 m^2\sin^2\theta &= \frac{1}{J_m H_m}\left[\cos^2\alpha\, H_m\partial_\rho J_m - \cos^2\theta\, J_m\partial_\rho H_m\right] \\ &\times \frac{1}{J_m H_m}\left[\cos^2\alpha\, H_m\partial_\rho J_m - n^2\cos^2\theta\, J_m\partial_\rho H_m\right] \\ &\equiv G^{TM}\cdot G^{TE}.\end{aligned} \tag{22}$$

Where we have defined:

$$\begin{aligned}G^{TE} &= \frac{1}{J_m H_m}\left[\cos^2\alpha\, H_m\partial_\rho J_m - n^2\cos^2\theta\, J_m\partial_\rho H_m\right] \\ G^{TM} &= \frac{1}{J_m H_m}\left[\cos^2\alpha\, H_m\partial_\rho J_m - \cos^2\theta\, J_m\partial_\rho H_m\right].\end{aligned} \tag{23}$$

This form is useful since the left-hand side is independent of k and vanishes as $\theta \to 0$ for all m, yielding

$$0 = G^{TE}\cdot G^{TM} = \left[H_m\partial_\rho J_m - n^2 J_m\partial_\rho H_m\right] \tag{24}$$
$$\times \left[H_m\partial_\rho J_m - J_m\partial_\rho H_m\right]. \tag{25}$$

The vanishing of the left bracket describes the resonance condition for the usual two-dimensional TE modes and the vanishing of the right bracket that for the TM modes,[10,13] so one recovers the correct limiting behavior as $\theta \to 0$ ($k_z \to 0$). In order to find the resonance wavevectors for the spiral modes at $\theta \neq 0$ one needs to find the complex roots of Eq. (22). An example of such solutions is given in Fig. 4, where the roots were found by the `SLATEC` routine `dnsqe`.[14] The series of resonances for a given value of m will be labeled by a second integer j which indexes the quantized radial momentum in the transverse plane.

Further insight into the solutions can be obtained by noting that for $k_z = 0$ and $m \neq 0$ the TE and TM resonance values differ so that at a typical TM resonance, for example, the factor G^{TE} will have its typical order of magnitude while the factor G^{TM} vanishes. By continuity of these functions with θ we can expect for small θ that the resonances will have one of the factors $G^{TM,TE}$ small while the other is not, and that the corresponding resonance will have a TM or TE character, i.e. the electric field will be predominantly in the z-direction or predominantly in the $x-y$ plane. The TE-like resonances will then show a large width (imaginary part) near the Brewster angle while the TM-like resonances will not. As the tilt angle θ increases the spiral modes become full mixtures of TE and TM modes and it is no longer possible to classify them in this manner. In Fig. 4, θ is small enough to classify them as TE- and TM-like and the coloring represents this classification.

Once the resonances are found, the polarization in the far field can be determined by rewriting Eq. (21) using the functions $G^{TM,TE}$ as

$$\xi_m = i\frac{m\left(n-n^3\right)\sin\theta}{n^2 G^{TE}}\alpha_m \tag{26}$$
$$\alpha_m = i\frac{m\left(n^3-n\right)\sin\theta}{n^2 G^{TM}}\xi_m. \tag{27}$$

The coefficients α_m, ξ_m determine the ratio of E_z to B_z in the far-field by

$$P = \frac{B_z^>}{E_z^>} = \frac{\xi_m}{\alpha_m} = i\frac{m\left(n-n^3\right)\sin\theta}{n^2 G^{TE}}. \tag{28}$$

We will however defer detailed analysis of the polarization properties of spiral resonances of the cylinder until

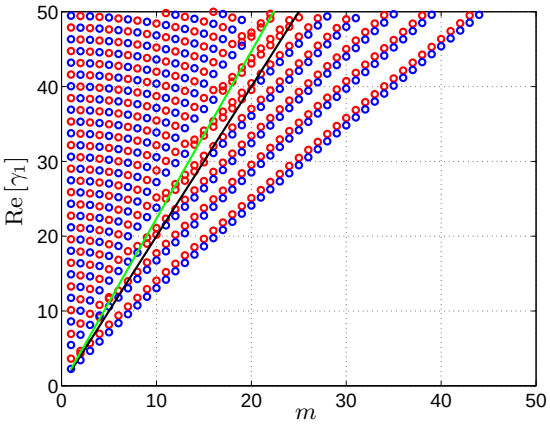

Fig. 4. TE like resonances (red circles) and TM like resonances (blue circles) for a cylinder with $n = 2, \theta = 0.2$, dashed line corresponds to the critical angle defined by $\gamma_1 = mn$ and the solid line to the Brewster condition $\gamma_1 = m\sqrt{n^2+1}$. Note that the TE or TM association does not work around the Brewster angle.

we have developed the theory in a more intuitive semi-classical approximation in Sections 5 below.

A. *Small θ expansion*

In the limit of small k_z, or θ, we see that Eq. (22) is of order θ^2 on the left hand side. Close to a TE or TM like resonance at $k = k_0$,$k_z = 0$, one of the factors G^{TE} or G^{TM} is small while the other is not. We expand the small term (which vanishes on resonance) to lowest order in θ^2 and insist that the resonance condition is satisfied at a slightly shifted value of the resonance wavevector, $nk = n(k_0 + \Delta k_0)$. One can then show that

$$\frac{\Delta k_0}{k_0} = \frac{1}{2}\alpha\theta^2 \tag{29}$$

where α is given by a ratio of Bessel functions, which is plotted in Fig. 5. Note that the coefficient $\alpha \approx 1$ for relatively small $\sin\chi$; exactly this value follows from the EBK quantization formula near normal incidence discussed in Section 5. This result can be compared to experiments done by Andrew Poon,[6] where a tilted optical glass fiber was illuminated with an unfocused Gaussian beam. A simple "wavefront matching" argument for this blue shift was given in Ref. 6 and is reproduced in Fig. 6. An incident plane wave propagates along the $X_{\rm lab}$ direction and is incident onto a rod tilted by an angle α. An upward propagating spiral resonance requires that the spiral wave be in phase with the incident wave farther up the tilted fiber. However upper incident wave of the same phase front must travel an extra distance d to reach the fiber when it is tilted. Thus the phase-matching condition between the internal wave and the extended incident wave reduces the effective cavity length for the spiral wave by a distance d/n, where n is the refractive index. Fixing

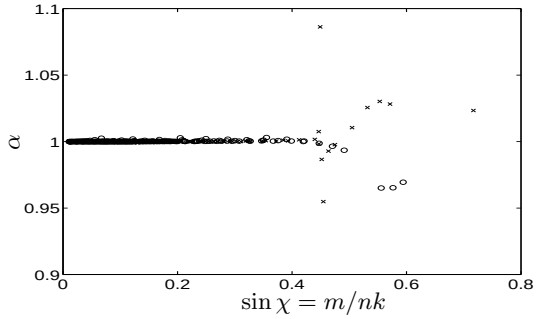

Fig. 5. Exact calculation of the coefficient for the resonant shift (circle) TM-like, (cross) TE-like. The coefficient is expected to be unity for small $\sin\chi$.

the quantum numbers of the resonances, this implies a quadratic blue-shift as a function of the tilt angle θ.

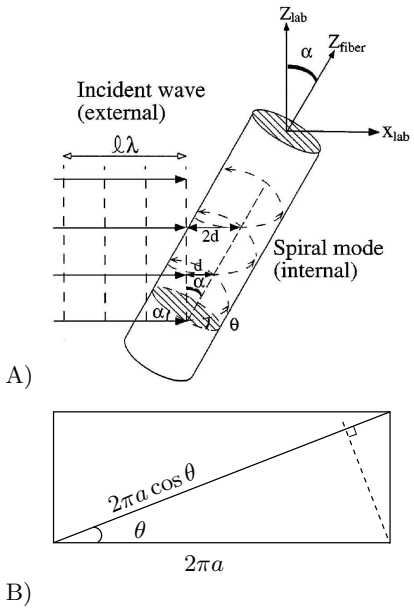

Fig. 6. A) Schematic of wave-front-matching argument. Internal spiral wave of a tilted optical fiber with respect to the incoming wave. The phase-matching condition between the spiral mode and the external incident wave reduces the effective cavity length for the spiral wave by a distance d/n, where n is the refractive index. B) The spiral quadratic blue shift can be interpreted by unwrapping the circular fiber. The dashed lines indicates the wavefront. The wavefront matched path is only $2\pi a\cos\theta$, therefore the resonances are quadratic blue shifted with the tilt angle. The figures are adapted from Poon.[6]

In Fig. 7 we compare the blueshift obtained from the exact numerical solution of Eq. (32) to the small θ expansion Eq. (29). The agreement is quite good. We will see at the end of the next section that the EBK quantization will give the same quadratic blue shift.

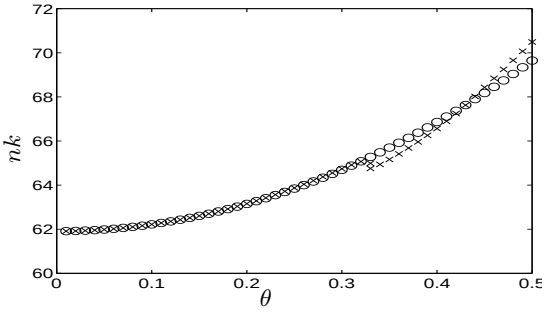

Fig. 7. Shift of the resonance condition with the quantum numbers $j = 21, m = 20$ ($\sin\chi \approx 0.33$) and $n = 2$ with respect to the internal tilt angle θ. Crosses are the numerical solutions following Eq. (32), and circles following the small θ expansion Eq. (29). Note the discontinuity in the exact numerical values around $\theta = 0.33$; this is due to the onset of the polarization critical angle which will be discussed in Section 7. This discontinuity occurs beyond the regime of the small θ expansion.

5. The EBK quantization conditions

As already noted, using the quantized solutions of resonance condition Eq. (22), we can easily calculate the polarization in the farfield. However, to get insight into the dependence of the polarization on the internal ray motion, a more appealing approach is to use the eikonal method, and the Einstein-Brillouin-Keller (EBK) type formulation of the resonance conditions. The eikonal method in general refers to finding approximate solution of the wave equation with a specific ansatz which is expected to be good in the short-wavelength limit ($k \to \infty$). The EBK method describes how to apply that ansatz to boundary value problems, typically assuming Dirichlet or Neumann boundary conditions.[15] The approach has been used for example to find approximate quantization formulas for the circular and elliptical billiard systems.[16] Recently it was generalized to treat the scalar Helmholtz equation for a dielectric billiard in two dimensions.[10] However it was also emphasized that the EBK method only works for the small subset of boundary shapes for which the ray motion within the boundary is integrable,[13] a point which goes all the way back to Einstein's original paper in 1917.[17] The motion of a ray within an infinite cylinder is also integrable (the energy and z-components of linear and angular momentum are conserved) and a generalization of the EBK method should work in this case also. The necessary generalization is to introduce the boundary conditions appropriate for the coupled E_z and B_z components of the field; this will lead to a generalization of the Fresnel coefficients for a plane interface.

We study the vector Helmholtz Equation (3) for $E_z(x,y), B_z(x,y)$ in the *semiclassical limit* $k, \gamma_{1,2} \to \infty$; in this limit we expect the solutions to have rapid phase variations and relatively slow amplitude variations. The generalized EBK ansatz for the quasi-bound solutions of the vector Helmholtz Eq. (3) can be written as

$$\begin{pmatrix} E_z \\ B_z \end{pmatrix} = \Psi(\boldsymbol{r}) = A_1 e^{i\gamma S_1(\boldsymbol{r})} + A_2 e^{i\gamma S_2(\boldsymbol{r})} \tag{30}$$

where $A_{1,2}$ are two-component vectors and S is the Eikonal. Note that all the functions are defined on the two-dimensional $x-y$ plane. Following Refs 10,16 we can write the general quantization condition

$$\gamma \oint_{\Gamma_i} d\boldsymbol{q} \cdot \nabla S = 2\pi l_i + \Phi_i \quad i = 1, 2. \tag{31}$$

Here the quantity ∇S is the gradient of the phase functions S_1, S_2 considered as the two sheets of a double valued vector field defined on the cross-section, l_i are integers and Γ_i refer to topologically irreducible set of loops. To avoid confusion in this section we temporarily drop the subscript $\gamma_1 \to \gamma$. Keller showed that in order for the EBK solution to be single-valued it is necessary that these loop integrals of the phase be quantized and that *any* two topologically inequivalent and non-trivial loops can be chosen. Φ_i is a total phase shift due to caustics and boundary scattering; for the scalar two-dimensional Helmholtz equation in a circle these phase shifts are known for Dirichlet, Neumann and dielectric boundary conditions. For the case of a dielectric circle the phase shifts are complex in general, representing either refraction out of the circle or the phase shift at the boundary due to total internal reflection.[10] In order to get the appropriate ray dynamics for the spiral modes it is easily shown that the eikonals S_1, S_2 must be identical to those of the two-dimensional circular billiard (i.e. $k_z = 0$); the new feature here is an additional eigenvalue condition on the amplitude two-vector, which will determine the eigenpolarization directions. This will lead to a modification of the phase shifts Φ_i with respect to the two-dimensional case.

Before discussing the latter point we briefly review the quantization relations assuming the Φ_i are known. Two conventional loops for implementing the quantization conditions are shown in Fig. 8. The first loop, Γ_1, goes just outside the inner turning point of a ray of fixed angular momentum; ∇S points in the direction of the ray so this integral just yields the length of the caustic for this ray. No caustic surfaces are crossed and the path does not touch the boundary, so the phase $\Phi_1 = 0$. Thus the first loop gives a relation equivalent to angular momentum conservation,

$$\sin\chi = \frac{m}{\gamma R} \tag{32}$$

where we have replaced the integer $l_1 \to m$ to conform to our earlier notation.

The second loop Γ_2 gives the quantization condition for the reduced wavevector γ in terms of the path length L of the loop (the vector field ∇S is everywhere parallel

to this path)

$$\gamma L = \left[2\cos\chi - 2\left(\frac{\pi}{2} - \chi\right)\sin\chi\right] R$$
$$= 2\pi j + \Phi_2, \tag{33}$$

where we have replaced the integer l_2 by j. This is exactly the relation we would find for the two-dimensional billiard problem, except that the transverse wavevector $\gamma = \sqrt{n^2k^2 - k_z^2}$ has replaced the full wavevector nk and the appropriate phase shift Φ_2 needs to be determined, and will differ from the two-dimensional case.

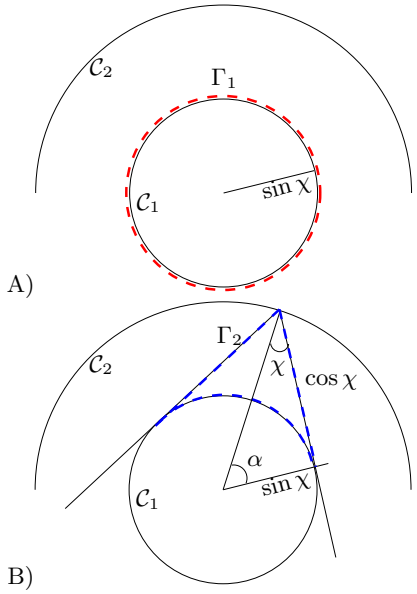

Fig. 8. A) Path of the first curve Γ_1. B) Second path Γ_2, of length L.

A. *Semi-classical boundary conditions for dielectric rod*

To treat the spiral modes of a dielectric cylinder in this approach we need to project the three-dimensional boundary conditions corresponding to Snell and Fresnel's laws into two dimensions. The relevant angles for this projection are all defined in Fig. 2 Since we are in the ray optics limit we can regard the "scattering" of the eikonal from the boundary as the scattering of a plane wave from the tangent plane. Because of our assumption of only outgoing waves, it is sufficient to assume only an incident, reflected and a transmitted wave (see Fig. 9).

1. Generalized Snell's law

The form of each of the fields is given by

$$\Psi^m = \begin{pmatrix} E_{z,m} \\ B_{z,m} \end{pmatrix} e^{i\gamma S_m}, \quad \text{with} \quad m \in \{i, r, t\} \tag{34}$$

The gradient of the Eikonal ∇S gives the direction of the the ray and is of constant length $|\nabla S| = n$. We find

$$\begin{array}{lll} \partial_n \boldsymbol{S}^i = i\gamma_1\cos\chi & \partial_n \boldsymbol{S}^r = -i\gamma_1\cos\chi & \partial_n \boldsymbol{S}^t = i\gamma_2\cos\sigma \\ \partial_t \boldsymbol{S}^i = i\gamma_1\sin\chi & \partial_t \boldsymbol{S}^r = \ \ i\gamma_1\sin\chi & \partial_t \boldsymbol{S}^t = i\gamma_2\sin\sigma \end{array}. \tag{35}$$

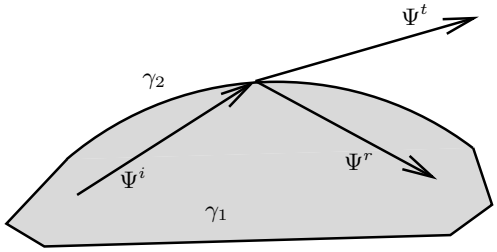

Fig. 9. Schematics of scattering on the projected plane. We will expand the wave solution inside into an incoming component Ψ^i and a reflected Ψ^r. The outside transmitted component is given by Ψ^t.

The first set of boundary conditions, the continuity of the field across the boundary, Eqs. (4) and (5) becomes:

$$\begin{pmatrix} E_z \\ B_z \end{pmatrix}^i e^{i\gamma_1 S^i} + \begin{pmatrix} E_z \\ B_z \end{pmatrix}^r e^{i\gamma_1 S^r} = \begin{pmatrix} E_z \\ B_z \end{pmatrix}^t e^{i\gamma_2 S^t}. \tag{36}$$

Since these equations need to hold everywhere on the boundary, the phases need to be equal, thus yielding

$$\gamma_1 S^i = \gamma_1 S^r = \gamma_2 S^t. \tag{37}$$

Using the fact that the tangent components are continuous, we obtain

$$\gamma_1 \sin\chi = \gamma_2 \sin\sigma \quad \Rightarrow \quad \sin\chi = \frac{\gamma_2}{\gamma_1}\sin\sigma. \tag{38}$$

This equation can be identified as the projection of *Snell's Law* into the transverse plane. Note that when $k_z = 0$ we recover the usual result

$$n\sin\chi = \sin\sigma. \tag{39}$$

We can write the projected Snell's Law in a completely geometric fashion noting $\gamma_1/\gamma_2 = \tan\theta/\tan\alpha$,

$$\sin\sigma = \frac{\gamma_1}{\gamma_2}\sin\chi = \frac{\sin\alpha\,\cos\theta}{\cos\alpha\,\sin\theta}\sin\chi = f(\theta) n \sin\chi. \tag{40}$$

With the function $f(\theta)$ given by

$$f(\theta) = \frac{\cos\theta}{\sqrt{1 - n^2\sin^2\theta}} = \sqrt{\frac{1-\sin^2\theta}{1-n^2\sin^2\theta}} \geq 1. \tag{41}$$

Hence, as is clear geometrically, the projected Snell's law, leads to total internal reflection of the projected motion before the critical angle $\sin\chi = 1/n$ is reached in the plane (this is simply because the actual angle of incidence is steeper than the projected angle due to the z-motion); the function $f(\theta)$ which determines the effective critical angle is plotted in Fig. 10.

2. Generalized Fresnel Matrices

The kinematics of the projected ray motion has been determined above simply from the continuity of the tangential components of the fields; the transport of ray

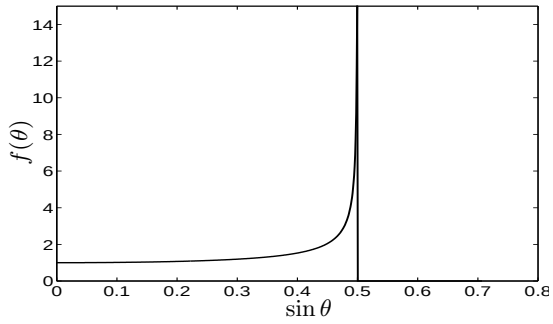

Fig. 10. Functional dependence of $f(\theta)$ for $n = 2$. Note that $f(\theta)$ diverges at the critical angle when $\sin\theta = 1/n$.

flux across the boundary will now be determined from the normal derivative boundary conditions.

$$\mathfrak{B}^i \begin{pmatrix} E_z \\ B_z \end{pmatrix}^i e^{i\gamma_1 S^i} + \mathfrak{B}^r \begin{pmatrix} E_z \\ B_z \end{pmatrix}^r e^{i\gamma_1 S^r} = \mathfrak{B}^t \begin{pmatrix} E_z \\ B_z \end{pmatrix}^t e^{i\gamma_2 S^t} \tag{42}$$

where the matrices $\mathfrak{B}$ are derived from the boundary conditions Eqs. (6) and (7) and given by the matrices

$$\mathfrak{B}^{(i,r)} = \begin{pmatrix} (n-n^3)\sin\theta\cdot\partial_t & \cos^2\alpha\cdot\partial_n \\ n^2\cos^2\alpha\cdot\partial_t & (n^3-n)\sin\theta\cdot\partial_n \end{pmatrix} \tag{43}$$

$$\mathfrak{B}^t = \begin{pmatrix} 0 & n^2\cos^2\theta\cdot\partial_n \\ n^2\cos^2\theta\cdot\partial_n & 0 \end{pmatrix}. \tag{44}$$

Here ∂_n and ∂_t are the normal and tangential derivatives. We can now relate the incoming field to the outgoing and the reflected using the boundary conditions Eq. (36) and Eq. (42)

$$\Psi^r = R\Psi^i \tag{45}$$

$$\Psi^t = T\Psi^i \tag{46}$$

where R and T are the general Fresnel matrices given by

$$R = \left(\mathfrak{B}^r - \mathfrak{B}^t\right)^{-1}\left(\mathfrak{B}^t - \mathfrak{B}^i\right) \tag{47}$$

and similarly

$$T = \left(\mathfrak{B}^t - \mathfrak{B}^r\right)^{-1}\left(\mathfrak{B}^i - \mathfrak{B}^r\right). \tag{48}$$

In the limit $\theta \to 0 \Rightarrow \alpha \to 0$ these 2×2 matrices become diagonal and take the form

$$R = \begin{pmatrix} \frac{n\cos\chi-\cos\sigma}{n\cos\chi+\cos\sigma} & 0 \\ 0 & \frac{\cos\chi-n\cos\sigma}{\cos\chi+n\cos\sigma} \end{pmatrix} \;\widehat{=}\; R = \begin{pmatrix} r_s & 0 \\ 0 & -r_p \end{pmatrix} \tag{49}$$

$$T = \begin{pmatrix} \frac{2n\cos\chi}{n\cos\chi+\cos\sigma} & 0 \\ 0 & \frac{2\cos\chi}{\cos\chi+n\cos\sigma} \end{pmatrix} \;\widehat{=}\; T = \begin{pmatrix} t_s & 0 \\ 0 & t_p \end{pmatrix}. \tag{50}$$

We recognize the diagonal elements as the Fresnel coefficients for TM (denoted by subscript s) and TE (subscript p) plane waves incident on a dielectric interface. The diagonal nature of the matrices implies that for $\theta = 0$ these polarization states are preserved. When $\theta \neq 0$ the matrices have off-diagonal elements implying the mixing of polarization states upon reflection (strictly speaking these matrices mix E_z and B_z upon reflection, which will be shown to be equivalent to rotating the local polarization). Recall that we are applying the EBK quantization condition (31) to the two-vector $(E_z(x,y), B_z(x,y))$; when we integrate around the path B in Fig. 8 which touches the boundary, we must impose the correct dielectric boundary conditions on this two-vector. In general this changes the ratio of E_z to B_z and will lead to a multi-valued solution as we complete the closed loop (for uniform index rods, only boundary scattering leads to the rotation of the two-vector). Therefore in order to have a single-valued solution the ratio of E_z to B_z must be unchanged upon reflection, i.e. the two-vector Ψ_i must be an eigenvector $\mathfrak{a}$ of the reflection matrix,

$$R\mathfrak{a} = \Lambda\mathfrak{a}. \tag{51}$$

We thus see that for the spiral modes of the cylinder there are two allowed mixtures of TM and TE polarization for each resonance labelled by angular momentum m and wavevectors γ_1, k_z; the eigenvalues of the R matrix $\Lambda = e^{i\eta}$ will give the extra phase shift Φ_2 needed to complete the EBK quantization condition in Eq. (33) ($\Phi_2 = \eta + \pi/2$ where the term $\pi/2$ comes from the caustic phase shift). As already shown above, at $\theta = 0$ the R matrix is diagonal, conventional TE and TM states are eigenvectors and the eigenvalues are just the Fresnel reflection coefficients, r_s, r_p. These have the familiar property of being purely real and less than unity for incident angle χ below total internal reflection, and complex numbers of modulus unity for angles above TIR. Hence one has pure reflection and refraction with no phase shift below TIR, and pure phase shift and no refracted wave above TIR. The phase shifts for totally internally reflected TM and TE waves are different and well-known functions of χ.[18] This familiar behavior is modified for the spiral modes.

The behaviour of the eigenvalues $\Lambda = e^{i\eta}$ of the matrix R for $k_z \neq 0$ is shown as a function of the angle $\sin\chi = m/\gamma$ in Fig. 11. Note that η is in general complex, and we are plotting here its magnitude. The magnitude of the eigenvalues are different up to a point between the Brewster angle (vertical dashed), and the CA (vertical dashed). At this point the the eigenvalues become complex conjugates of each other. We will call this point, the *polarization critical angle* (PCA) and will explain how it is related to the far-field polarization below. Hence spiral modes acquire a phase shift upon reflection before they reach the critical angle. Not until the CA do $\Lambda_{1,2}$ lie on the complex unit circle as they should for TIR. Thus we have a new phenomenon, a phase shift for a refracted wave. Having determined the two possible values of Φ_2, we can write the quantization condition for the spiral

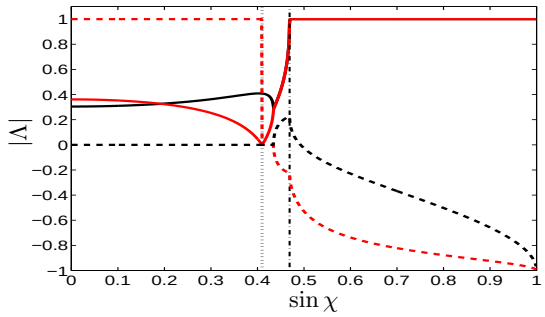

Fig. 11. Absolute value (solid red and black lines) and the phase divided scaled by π (dashed red and black lines) of the eigenvalues of R for $n = 2$ and $\tan\theta = 0.2$ vs. $\sin\chi$. The dotted black horizontal line is the Brewster angle and the black dashed line is the critical angle. Red indicates the TE-like component and blue the TM.

resonances as a transcendental equation

$$2\gamma\sqrt{1-\frac{m^2}{\gamma^2}}+2m\arcsin\left(\frac{m}{\gamma}\right)=2\pi j+\frac{\pi}{2}+m\pi+\zeta+i\ln|r|, \tag{52}$$

where j, m are integers, $\Lambda = re^{i\zeta}$, and we have used the angular momentum quantization condition Eq. (32). We can simplify this result further to get an explicit solution for rays near normal incidence in the plane, so that $\sin\chi \to 0$:

$$\gamma = \pi\left[j+\frac{m}{2}+\frac{1}{4}\right]+f(\chi,\theta) \tag{53}$$

where the contributions of the phase shift and the loss at the boundary have been combined in $f(\chi)$. We will analyze the function $f(\chi,\theta)$ further in the next section on polarization properties of the spiral modes.

From Eq. (53) we can derive the blue shift for small θ by noting the the right hand side without $f(\chi,\theta)$ is just the resonant condition for the circle. From the definition of $\gamma = \sqrt{nk^2 - k_z^2} = nk(1-\sin^2\theta)$ we can write

$$nk = nk_o\left(1+\frac{1}{2}\theta^2\right), \tag{54}$$

where nk_o is the resonance condition for the circle $\theta = 0$. Comparing to Eq. (29) above we see that this implies that the coefficient of the small θ quadratic blue-shift should be $\alpha = 1$ for small $\sin\chi$, just as we found in Fig. 5 above. As noted there, this coefficient changes slightly when the polarization critical angle is reached; this change is captured by the contribution from $f(\chi,\theta)$ we have just neglected. In Tab. 1 we compare the resonances found by the exact wave matching method (Eq. (22)) and by the EBK method finding good agreement for $\theta = 0.1, 0.2$.

In general we can always calculate the R matrix via Eq. (47), find the eigen-polarization directions, and subsequently act with T on the internal eigen-polarizations

Table 1. spiral resonances of the cylinder with $n = 2, \theta = 0.1, 0.2$. We compare the resonances calculated by the solution of Eq. (22) and the EBK method, finding good agreement. Although resonances can no longer be classified as TM or TE, classification as TM-like or TE-like is based on which factor $G^{TE,TM}$ is small at the resonance as discussed above

$\theta = 0.1$		exact		EBK
m		kR	j	kR
18	TE	100.52083-0.27170i	55	100.520468-0.271695i
20	TE	100.42571-0.27098i	54	100.425346-0.270979i
44	TE	100.06672-0.25117i	43	100.066168-0.255107i
74	TE	100.30341-0.20475i	31	100.301095-0.204629i
98	TE	101.41861-0.09114i	23	101.382400-0.075236i
$\theta = 0.2$				
5	TM	99.62235-0.59423i	29	99.61990-0.59421i
17	TE	99.86057-0.55418i	23	99.86699-0.55433i
20	TM	99.29851-0.56992i	22	99.29473-0.56984i
34	TE	100.17837-0.84848i	16	100.20152-0.85155i
39	TE	99.78148-1.35232i	14	99.74088-1.36053i
57	TE	99.76787-0.00005i	8	96.79993+0.00009i
62	TM	100.78974-0.00000i	7	100.86339+0.00000i

to determine the corresponding polarization in the far-field. A physically more transparent method to do this involves the a reformulation of the problem in terms of the actual polarization vector, rather than the two-vector (E_z, B_z). Below, we will introduce an equivalent matrix description in terms of the Jones Algebra which we will subsequently show to be exactly equivalent to the (E_z, B_z) description.

6. Jones formulation of polarization properties

We introduce the parallel and perpendicular components of the electric field, E_p and E_s in the local coordinate system defined by the plane of incidence. The Jones vector[19] which describes the local polarization is

$$\boldsymbol{E} = \begin{pmatrix} E_p \\ E_s \end{pmatrix} = \begin{pmatrix} E_{0p}e^{i\phi_p} \\ E_{0s}e^{i\phi_s} \end{pmatrix} \tag{55}$$

with E_{0s} and E_{0p} being the magnitude of the electric field and the phases ϕ_s and ϕ_p. The Jones matrix for the reflection and transmission at a dielectric interface is give by

$$J_r = \begin{pmatrix} -r_p & 0 \\ 0 & r_s \end{pmatrix} \quad \text{(for reflection)}, \tag{56}$$

$$J_t = \begin{pmatrix} t_p & 0 \\ 0 & t_s \end{pmatrix} \quad \text{(for transmission)} \tag{57}$$

and would describe any series of reflection in the same plane of incidence. However a spiraling ray in the cylinder changes its plane of incidence at each reflection, so

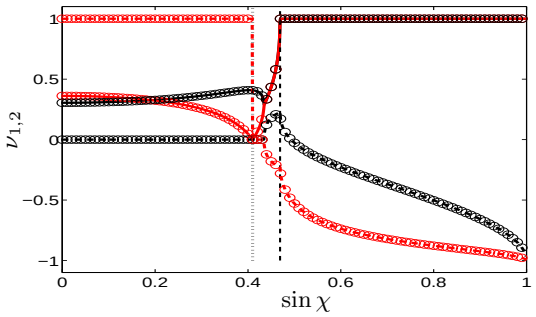

Fig. 12. Comparison of the of the eigenvalues of the rotated Jones matrix, absolute value (solid line red/black) and the phase (divided by π) (dashed line red/black), to the eigenvalues of R (red/black circles). Parameters of the calculation are $\tan\theta = 0.2$ and $n = 2$.

that we need to rotate our coordinate system into the new plane of incidence between each reflection before we apply the Jones reflection and transmission matrices. (It is precisely this rotation of the plane of incidence for a spiraling ray which is the physical reason behind the non-conservation of TE or TM polarization). If the angle between the two planes is given by ξ we can do this by multiplying the Jones vector by the rotation matrix $\Re(\xi)$. This angle ξ can be determined for a general cylindrical symmetry.[11] Due to the rotational and translational symmetry of the cylinder, the polarization at each angle ϕ on the cylinder must be the same for any value of z and must be described by the same Jones vector when referred to the plane of incidence at that point. Therefore the Jones vector emerging from a reflection must be the same as the incident Jones vector once the coordinate system has been rotated into the new plane of incidence. This yields an eigenvalue condition for the Jones vectors describing the spiral modes of the cylinder,

$$\mathfrak{J}\begin{pmatrix} E_p \\ E_s \end{pmatrix}_{1,2} = \nu_{1,2}\begin{pmatrix} E_p \\ E_s \end{pmatrix}_{1,2} \tag{58}$$

where $\mathfrak{J} = \Re(\xi)J_r$. Thus the two polarization states are the two eigenvectors of $\mathfrak{J}$ and their eigenvalues $\nu_{1,2}$ describe the phase shifts and refractive losses at each reflection, just as do the eigenvalues of R for the two-vector E_z, B_z studied earlier. Therefore, the two matrices $\mathfrak{J}$ and R are related by a similarity transformation and have the same eigenvalues[11] which is confirmed in Fig. 12.

7. Polarization critical angle

Realizing that the eigenvalues of interest are obtained from the product a rotation and a diagonal Jones matrix with known entries allows us to understand the behavior of the these eigenvalues rather simply. The eigenvalues can now be written in terms of the rotation angle of the plane of incidence, ξ and the Fresnel reflection coefficients

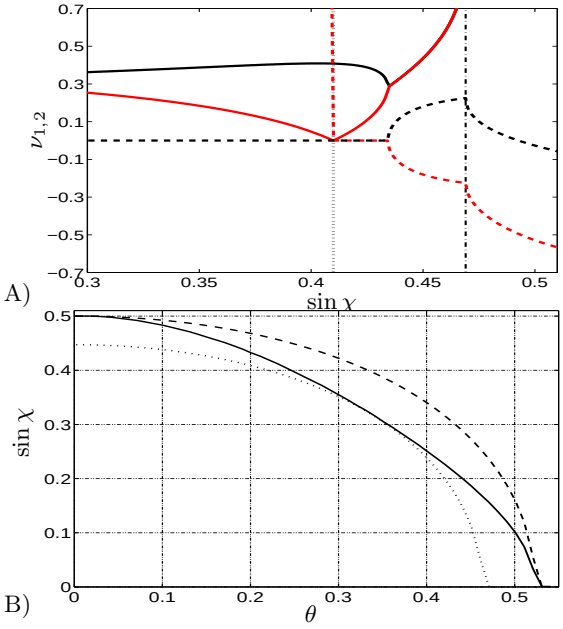

Fig. 13. A) Absolute value of the two eigenvalues $\nu_{1,2}$ of the rotated Jones matrix (solid red and black). Phase of the eigenvalues (divided by π) is plotted in dashes. The Eigenvalues become complex at the point where the two curves meet and join. This point lies between the Brewster angle (dashed vertical black) and the effective critical angle (dotted vertical black). Calculated for $\tan\theta = 0.2$, $n = 2$. B) (Black) The sine of the polarization critical angle PCA at which the eigenvalue of R gets complex. (Dotted) Sine of the Brewster Angle, (Dashed) sine of the critical angle of total internal reflection.

r_s, r_p,

$$\nu_{1,2} = \frac{1}{2}\cos\xi\,(r_s - r_p) \pm \frac{1}{2}\sqrt{\cos^2\xi\;(r_s - r_p)^2 + 4r_p r_s}. \tag{59}$$

Consider the discriminant of the eigenvalues, $D = \cos^2\xi\,(r_s - r_p)^2 + 4r_s r_p$, which determines whether they are real or complex. Recall that the TM Fresnel reflection coefficient, r_s is real and positive for all angles below the critical angle passing through unity and becoming complex and unimodular above the critical angle; whereas the TE reflection coefficient, r_p is real below the critical angle but becomes negative at the Brewster angle and passes through negative one before becoming unimodular and complex above the critical angle. It follows that D will always be positive and $\nu_{1,2}$ real for angles of incidence below the Brewster angle. However for any non-zero value of the rotation angle ξ, D will become zero *before* the critical angle since at the critical angle $D = 4(1 - \cos^2\xi)$ is negative. The value of the incidence angle ξ when $D = 0$ is the polarization critical angle (PCA) which we have already mentioned above. Since it occurs when both r_s, r_p have absolute value less than unity, the eigenvalues $\nu_{1,2}$ also have modulus less than unity and we have a phase shift upon reflection while a

fraction $1-|\nu_{1,2}|^2$ of the incidence wave is refracted out. This fraction can be calculated and does not correspond to either of the usual Fresnel transmission coefficients for TM or TE. The behavior of the eigenvalues just described is shown in Fig. 13 A); the behavior of the polarization critical angle vs. $\sin\chi$ is shown in Fig. 13 B). We see that for small θ the onset of the the phase shift is close to the critical angle (CA); as θ varies the PCA moves close to the Brewster angle and then for θ close to the CA, where for any $\sin\chi$ we will have TIR, the PCA returns to the CA. This analysis allows us a simple understanding of why there is a PCA which precedes total internal reflection. The TM and TE components of the spiral resonances have no relative phase shift at reflection until the Brewster angle; at the Brewster angle the TE component picks up a π phase shift, which mixes with the TM component to give a phase shift between zero and π. Right at the Brewster angle r_p vanishes and the local TE component of the resonance is filtered out, but as the TE reflectivity picks up above the Brewster angle this phase shift appears before total internal reflection condition is reached. It is interesting to note that due to the finite phase aquired at the PCA, the resonance condition Eq. (53) is slightly changed. The term PCA suggests that at this angle the polarization properties of the spiral modes change. We shall see that this is the case in the next section.

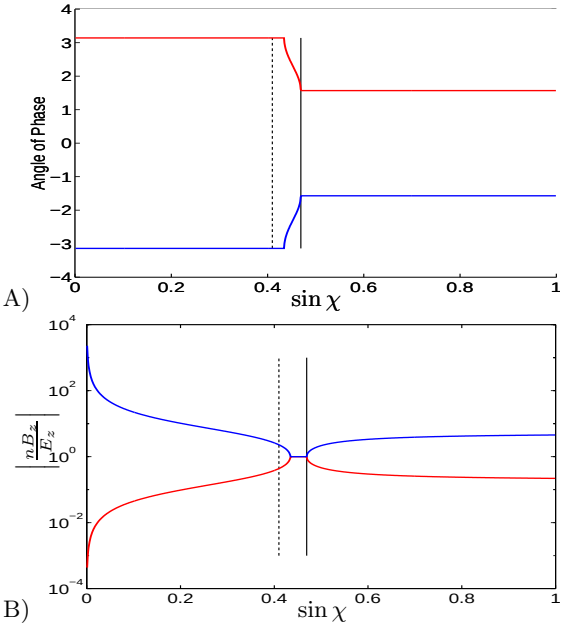

Fig. 14. A) Phase differences between the E_z and B_z field, for TE and TM like modes. B) Absolute values of the ratio of the eigenvector components of R. For normal incidence $\sin\chi = 0$ the modes are clearly either TE or TM, right at the PCA they completely mix. Calculations done for $n = 2$, $\tan\theta = 0.2$. The solid vertical black line is the effective critical angle, the dashed line the effective Brewster angle.

8. Polarization properties of spiral modes

When the eigenvalues of the $\mathfrak{J}$ matrix are real, the eigenvectors can be chosen real (up to an overall phase) and thus there is no relative phase shift between E_s and E_p. While in general polarization is not well-defined inside the dielectric, in the short wavelength limit we are now examining it is well defined with respect to the considered ray direction, and zero relative phase shift implies linear polarization of the resonance with respect to the spiraling ray direction. Above the PCA, when the eigenvalues are complex, the eigenvectors also become complex and there is a relative phase shift between E_s and E_p corresponding to elliptical polarization of the internal field. This picture is confirmed by the calculation of the eigenvalues plotted in Fig. 14 A), B). At small $\sin\chi$ we have a large ratio between the eigenvector components and zero phase shift, corresponding to linear polarization with the electric field almost completely in the z or transverse direction (TM-like and TE-like). After the PCA we get a phase shift approaching $\pi/2$ and equal ratios leading to circular polarization right at the CA; above the CA we have in general elliptical polarization for the internal fields with a calculable ellipticity and with a phase difference of $\pi/2$ as expected for whispering gallery modes.

The far-field polarization arising from this internal field can be found by applying to the relevant eigenvector of $\mathfrak{J}$ the transmission matrix J_t and then rotating the resulting vector by an angle Θ which projects the Jones vector onto the the plane perpendicular to the outgoing ray direction discussed in Section 6 above. This angle Θ can be determined by straightforward geometric considerations which we omit here and simply state that the the far-field polarization vector (E'_s, E'_p) is given by

$$\mathfrak{R}(-\Theta)J_t|\mathfrak{a}\rangle \tag{60}$$

where $\mathfrak{R}$ is the the rotation just mentioned and $|\mathfrak{a}\rangle$ is either of the eigenpolarization vectors of $\mathfrak{J}$.

In Fig. 15 A), B), we compare the far-field polarization states for spiral resonances of the cylinder as predicted by the exact and geometric optics approach. We find good agreement between the methods, although the exact solutions smooth the abrupt behavior near the PCA predicted by the geometric optics approach. Above the CA we have only evanecent emission, but the eccentricity of the two-vector is still finite. Note that as formulated, the Jones approach gives a continuous solution for the two polarization states, whereas the exact resonances are discrete and correspond to discrete allowed angles χ which can be also found through the EBK approach. The Jones approach provides a smooth and k-independent formula for the polarization states which agress with those of the resonaces.

9. Summary and conclusions

We have reduced the Maxwell's equations for a dielectric rod of arbitrary cross-section to a vector Helmholtz

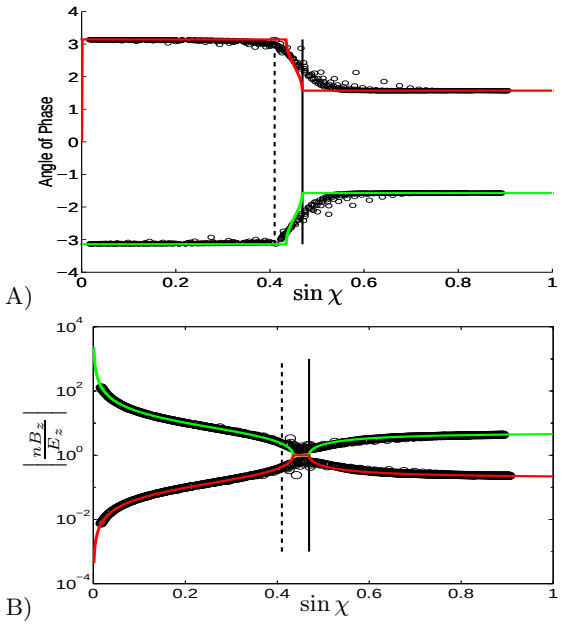

Fig. 15. Respective A) phase differences and B) absolute values of the ratio of the eigenvector components of R (green and red solid) in the farfield. The black circles are the exact numerical solutions following Eq. (22) ($m \in [0, 50]$ and $\gamma_1 < 50$). For $n = 2$, $\tan\theta = 0.2$. The solid vertical black line is the effective critical angle, the dashed line the effective Brewster angle.

equation for a two-component vector field living in the two-dimensional cross-sectional plane. We have devised a formulation of the resonance problem for the quasi-bound modes (spiral resonances), which can be implemented numerically for a general cross-section, and shown how the polarization state of the resonances in the farfield can be determined. Calculations were reported for the case of a circular cross-section (cylinder) and the results were compared to ray-optical results from an EBK formulation of the resonance problem in the semi-classical limit. We have analyzed the polarization state of the spiral resonances both inside the cylinder and in the farfield, and related its properties to the internal ray motion. It was shown that as the tilt angle of the spiraling ray with respect to the cross-sectional plane is increased, there exists a polarization critical angle at which the polarization changes from linear to elliptical both internally and externally and this occurs before the total internal reflection condition, so the effect can be measured readily in the far-field. The physical picture we developed in terms of the Jones polarization vectors was useful in understanding the PCA and may be useful in generalizing the analysis to arbitrary cross-sections for which the ray motion can be chaotic.

Acknowledgments

We would like to thank Richard Chang and Andrew Poon for usefull discussions and greatfully acknowledge support from the National Science Foundation grant DMR-0408638.

References

1. C. Gmachl, F. Capasso, E. E. Narimanov, J. U. Nöckel, A. D. Stone, J. Faist, D. L. Sivco, and A. Y. Cho. High-power directional emission from microlasers with chaotic resonators. *Science*, 280:1556–1564, 1998, cond-mat/9806183.
2. J. U. Nöckel and A. D. Stone. Ray and wave chaos in asymmetric resonant optical cavities. *Nature*, 385:45–47, 1997, chao-dyn/9806017.
3. N. B. Rex, H. E. Tureci, H. G. L. Schwefel, R. K. Chang, and A. D. Stone. Fresnel filtering in lasing emission from scarred modes of wave-chaotic optical resonators. *Phys. Rev. Lett.*, 88:art. no. 094102, 2002, physics/0105089.
4. G. D. Chern, H. E. Tureci, A. D. Stone, R. K. Chang, M. Kneissl, and N. M. Johnson. Unidirectional lasing from InGaN multiple-quantum-well spiral-shaped micropillars. *Appl. Phys. Lett.*, 83:1710–1712, 2003.
5. Harald G. L. Schwefel, Nathan B. Rex, Hakan E. Tureci, Richard K. Chang, A. Douglas Stone, Tahar Ben-Messaoud, and Joseph Zyss. Dramatic shape sensitivity of directional emission patterns from similarly deformed cylindrical polymer lasers. *J. Opt. Soc. Am. B*, 21:923–934, 2004, physics/0308001.
6. A. W. Poon, R. K. Chang, and J. A. Lock. Spiral morphology-dependent resonances in an optical fiber: Effects of fiber tilt and focused Gaussian beam illumination. *Opt. Lett.*, 23:1105–1107, 1998.
7. J. A. Lock. Morphology-dependent resonances of an infinitely long circular cylinder illuminated by a diagonally incident plane wave or a focused Gaussian beam. *J. Opt. Soc. Am. A*, 14:653–661, 1997.
8. G. Roll and G. Schweiger. Resonance shift of obliquely illuminated dielectric cylinders: geometrical-optics estimates. *Appl. Opt.*, 37:5628–5630, 1998.
9. Harald G. L. Schwefel and A. Douglas Stone. Vector resonances in chaotic dielectric rods. *in progress*, 2005.
10. Hakan E. Türeci. *Wave chaos in dielectric resonators: Asymptotic and numerical approaches*. PhD thesis, Yale University, New Haven, USA, 2003.
11. Harald G. L. Schwefel. *Directionality and Vector Resonances of Regular and Chaotic Dielectric Microcavities*. PhD thesis, Yale University, New Haven, USA, 2004.
12. T. Harayama, P. Davis, and K. S. Ikeda. Stable oscillations of a spatially chaotic wave function in

a microstadium laser. *Phys. Rev. Lett.*, 90:063901, 2003.

13. H. E. Tureci, H. G. L. Schwefel, Ph. Jacquod, and A. Douglas Stone. Modes of wave-chaotic dielectric resonators. *Progress In Optics*, 47, 2005, physics/0308016.
14. SLATEC. SLATEC Common Mathematical Library (Version 4.1), July 1993. `http://www.netlib.org/slatec/`.
15. J. B. Keller. Corrected Bohr-Sommerfeld quantum conditions for nonseparable systems. *Ann. Phys.*, 4:180–188, 1958.
16. J. B. Keller and S. I. Rubinow. Asymptotic solution of eigenvalue problems. *Ann. Phys.*, 9:24–75, 1960.
17. A. Einstein. Zum Quantensatz von Sommerfeld und Epstein. *Verhandl. Deut. Physik. Ges.*, 19:82–92, 1917.
18. J. D. Jackson. *Classical electrodynamics*. John Wiley & Sons, Inc., New York, USA, 1998.
19. R. C. Jones. A new calculus for the treatment of optical systems. I. description and discussion of the calculus. *J. Opt. Soc. Am.*, 31:488–493, 1941.